VI. Conclusions

The experimental findings for SiH_3^+, SiH_3, and SiH_3^- are completely in accord with the qualitative ideas outlined in Figure 1. The SiH_3^- photodetachment spectra can be adequately modeled by using a single oscillator to describe the active mode in both the initial anion and the final silyl radical. The parameters for these umbrella potentials are found by choosing values which best fit the SiH_3^- spectrum (Figure 3). These potentials then accurately predict the SiD_3^- spectrum found in Figure 5. We have endeavored to "check" our potential for SiH_3 (derived from the SiH_3^- photoelectron spectra) by "predicting" the Franck-Condon profile of the SiH_3 photoionization spectrum: $SiH_3^+ \leftarrow SiH_3$. One's general ideas about valence (Figure 1) suggest that the umbrella potential for SiH_3^+ is a simple oscillator with a single minimum at $\xi_0 = 0°$; we appeal to the experiments outlined in ref 15 to establish that the umbrella oscillator for SiH_3^+ is a simple, linear oscillator with $\omega_2 = 820$ cm^{-1}. Our simulation of the SiH_3 photoionization spectrum is depicted in Figure 11 and fits the experimental findings.[15]

A summary of experimental properties is presented in Table V. The electron affinities, ionization potentials, vibrational frequencies (except for SiD_3^+), and heats of formation are all measured directly. Most of the molecular constants such as the inversion barrier, α(H–Si–H), and the rotational constants (B and C) are extracted from modeling experimental data. The accuracy of the silyl radical constants has recently been dramatically improved by the completion of an infrared diode laser absorption study.[50] This study reports the following values for SiH_3: α(H–Si–H) = 110.5°, r_0(Si–H) = 1.468 Å, and B ($v'' = 0$) = 4.763 15 cm^{-1}. The SiH_3 inversion barrier is estimated to be 1868 cm^{-1}. Our negative ion photoelectron results agree with these more precise values.

Acknowledgment. This paper is dedicated to Professor Peter P. Gaspar in honor of his award of the Frederic Stanley Kipping Award in Organosilicon Chemistry. We have had fruitful conversations with J. G. Radziszewski, J. Michl, and P. R. Bunker. We thank K. E. Salomon and J. I. Brauman for a preprint of their SiH_3^- photodetachment paper and for pertinent discussions. This work was supported by the U. S. Department of Energy (Contract No. DE-AC02-80ER10722). The VAX 11/750 digital computer used to carry out the Franck-Condon factor calculations was acquired with the help of the National Science Foundation CHE-8407084).

Registry No. SiH_4, 7803-62-5; SiH_3^-, 15807-96-2; SiD_3^-, 54637-68-2; SiH_3, 13765-44-1; SiD_3, 69103-84-0; NH_3, 7664-41-7.

Metal Cluster vs. Atom Reactivities. Calcium and Magnesium Vapor with Alkyl Halides and Methane

Kenneth J. Klabunde* and Alan Whetten

Contribution from the Department of Chemistry, Kansas State University, Manhattan, Kansas 66506. *Received April 4, 1986*

Abstract: Vapors of calcium and magnesium were codeposited with argon and argon/CH_3X mixtures (X = I, Br, Cl, F, H) at 9 K. Growth rates for Ca, Ca_2, Ca_x, Mg, Mg_2, Mg_3, Mg_4, and Mg_x in the presence and absence of CH_3X were monitored and reactivity trends established showing (a) clusters were more reactive than atoms, (b) larger clusters were more reactive than smaller clusters, (c) calcium species were more reactive than magnesium species, and (d) the reactivity trend for CH_3X was $CH_3I > CH_3F > CH_3Br > CH_3Cl$. Thermodynamic and ionization potential considerations seem to explain these trends.

We are interested in directly comparing chemical reactivities of ground-state atoms of the elements, and in comparing reactivities of small metal clusters with atoms. Recently we reported that Mg_2 and Mg_3 exhibited reactivity toward CH_3Br but Mg atoms did not.[1] Matrix isolation studies at low temperature sometimes allow such direct reactivity comparisons under exactly the same conditions of temperature, pressure, and concentration. Herein we report more complete studies on calcium and magnesium.

Background and Results

Calcium. The absorption spectra of calcium vapor species codeposited with inert gases have been studied in several laboratories.[2-4] Although there has been some disagreement over peak assignments, it is well-established that there is a strong atomic absorption due to the $4s4p \leftarrow 4s^2$ transition ($^1P_1 \leftarrow {}^1S_0$) near 410 nm (in argon). This transition appears as an asymmetric doublet corresponding to the 422.7-nm atomic transition in the gas phase. The splitting of this atomic band may be due to the non-O_h symmetry of the lattice causing a vacancy to be present next to the metal atom.[3] A sharp transition at 456 nm has been assigned as a forbidden $^1D_2 \leftarrow {}^1S_0$ atomic Ca transition.[2] It has been suggested that the symmetry of an incompletely substituted matrix site or a site containing a nearby impurity is reduced such that ^1P and ^1D have a common irreducible representation of approximately D_{3h} symmetry. Upon lowering the symmetry (from O_h), these two states can mix to give some observable intensity to the forbidden transition.[2]

Table I. UV–Visible Spectral Assignments for Matrix-Isolated Calcium Atoms, Dimers, and Clusters in Argon[a]

wavelength (nm)	species	assignment	ref
374	Ca_2	$^1\pi_u \leftarrow {}^1\Sigma_g^+$	5
415	Ca	$4s4p\ ^1P_1 \leftarrow 4s^2\ ^1S_0$	2,3
448[b]	Ca	$^1D_2 \leftarrow {}^1S_0$	2
470	Ca_x		
505	$Ca_x + Ca_2$		
550	Ca_x		
648	Ca_2	$1\Sigma_u^+ (^1S + {}^1P) \leftarrow {}^1\Sigma_g^+ (^1S + {}^1S)$	7

[a] These are the bands observed in this work. Assignment are based on literature cited. [b] This band is questionable and we suspect it is not due to the atom. It was not considered for our reactivity comparisons.

(1) Imizu, Y.; Klabunde, K. J. *Inorg. Chem.* **1984**, *23*, 3602–3605.
(2) Andrews, L; Duley, W. W.; Brewer, L. *J. Mol. Spectrosc.* **1978**, *70*, 41–52.
(3) Francis, J. E., Jr.; Webber, S. E. *J. Chem. Phys.* **1972**, *56*, 5879–5886.
(4) Brewer, L.; Wang, J. L. F. *J. Chem. Phys.* **1972**, *56*, 4305–4309.

0002-7863/86/1508-6529$01.50/0

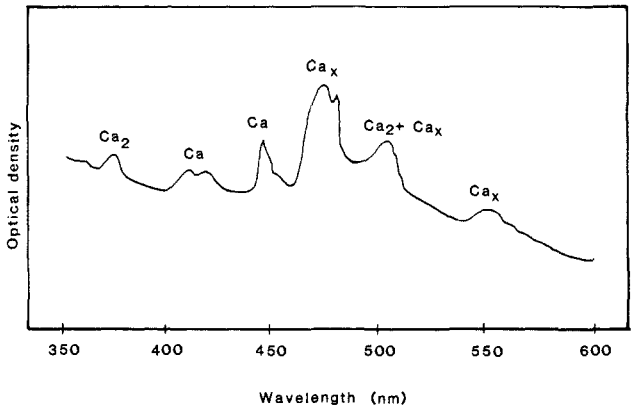

Figure 1. Absorption spectrum of calcium species isolated in frozen argon.

The dimeric calcium species has been extensively studied in inert gas matrices.[5-8] This Ca_2 species has generated specific interest since the bonding is attributed wholly to the van der Waals interactions between the two Ca atoms.[6] The electronic configuration of the dimer shows an equal number of bonding and antibonding electrons resulting in no formal bonding in the ground state $[(\sigma_g 4s)^2(\sigma_u 4s)(\sigma_g 4p)]$.[7] One study shows a 12-membered band with 113-cm^{-1} spacings centered at 648 nm assigned as the $^1\Sigma_g^+(^1S\,^1S) \rightarrow {}^1\Sigma_u^+(^1S + {}^1P)$ transition.[8] Two additional weaker absorptions have been observed at 500 and 374 nm, and there are indications that the 500-nm band may be overlapping with an absorption for a higher aggregate Ca_x found at 484 nm.[5]

Turning to our results, Figure 1 shows a typical spectrum obtained when we codeposited Ca vapor with argon on a KBr window at 9 K. Table I summarizes the bands we observed. Some of our peaks are broader than other workers have found; we attribute this to matrix effects where absorptions from nonequilibrium (multiple) lattice sites tend to broaden a transition line. For our work higher spectral resolution was not a requirement. We also observed that the bands due to atomic transitions were usually weaker than those due to clusters. This was a result of our higher metal vapor flux and the use of argon gas, allowing more diffusion and metal aggregation, which was beneficial for our work since we were particularly interested in the clusters.

Note from Figure 1 that the atomic Ca (P ← S) band appears as an asymmetric doublet centered at 415 nm. A second forbidden atomic transition (D ← S) is at 448 nm. We feel this assignment is questionable. Note the large size of the 448-nm band. Earlier reports[2,5] indicate that this transition should only be about 4% the size of the 415-nm absorption, yet our results show this 448-nm band to be 15–45% the size of the 415-nm band. Also, these two atomic transitions are affected differently by the presence of CH_3X, and, in fact, its chemical reactivity behavior exactly mimics that of dimers and clusters. Thus, we believe the 448-nm band is not due to atoms. At any rate, it is not considered further since the other bands with more certain assignments were adequate for our needs.

Figures 2, 4, and 5 illustrate how certain absorptions change with time in the presence of pure argon vs. a mixture of argon plus a small amount of CH_3X (0.6%). Each plot shows the absorption area of each indicated peak vs. deposition time. Throughout the entire experiment Ca vapor flux remained constant and gas flow rate remained constant. The only variable was gas composition, that is, a switch from pure Ar (labeled A) to Ar/CH_3X (labeled B). We refer to this as matrix gas switching. The final part of each plot shows what happens to the bands upon annealing for 10 min at 25–35 K. Note that two different scales are used on the plots, and are indicated by arrows.

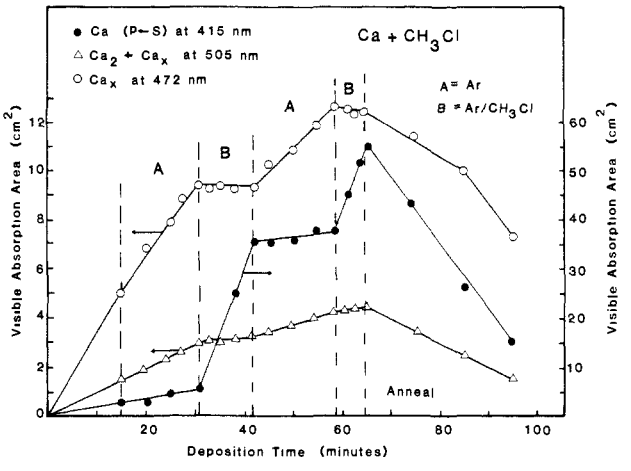

Figure 2. Absorption areas vs. time for calcium species in argon (A) vs. argon/CH_3Cl (B).

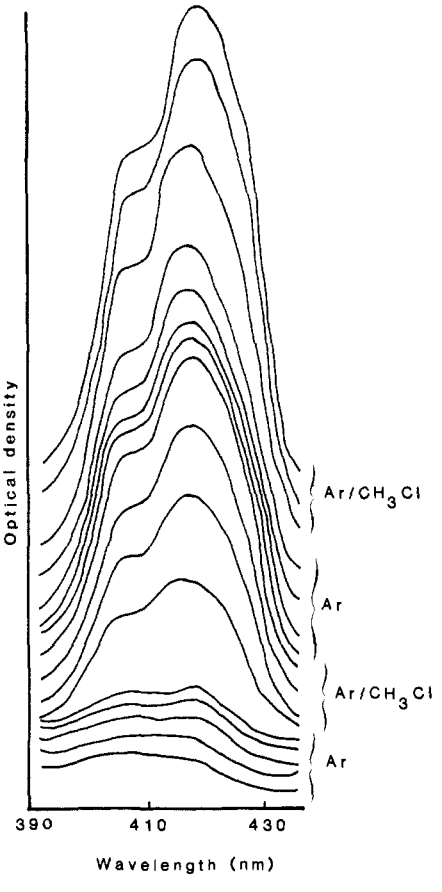

Figure 3. Calcium atom (P ← S) band growth in argon and argon/CH_3Cl.

Calcium/CH_3Cl. Inspection of Figure 2 shows that atoms and cluster species behaved quite differently in the presence of CH_3X. In pure Ar all bands grew at constant rates. Upon switching to Ar/CH_3Cl there was a dramatic increase in the growth rate of the 415-nm P ← S atomic line; the area under this peak was enhanced 400% within 4 min! At the same time, however, the area under the bands due to Ca_x (472 nm) and Ca_2 (505 and 374 nm) stopped growing and even decreased slightly (the 505- and 374-nm bands behaved identically in all of our studies; although the 505-nm band is due to Ca_2, its area is affected by the large adjacent 472-nm Ca_x band, and therefore the plots show the 505-nm band as $Ca_2 + Ca_x$). Upon switching to pure Ar again, original growth patterns were established. Upon switching to Ar/CH_3Cl again, the same results as before were observed; and upon annealing, relatively constant decreases of all bands were observed.

(5) Miller, J. C.; Mowery, R. L.; Krausz, E. R.; Jacobs, S. M.; Kim, H. W.; Schatz, P. N.; Andrews, L. *J. Chem. Phys.* **1981**, *74*, 6349–6361.
(6) Balfour, H. J.; Whitlock, R. F. *Chem. Commun.* **1971**, 1231.
(7) Miller, J. C.; Andres, L. *Chem. Phys. Lett.* **1977**, *50*, 315–319.
(8) Miller, J. C.; Ault, B. S.; Andrews, L. *J. Chem. Phys.* **1977**, *67*, 2478–2487.

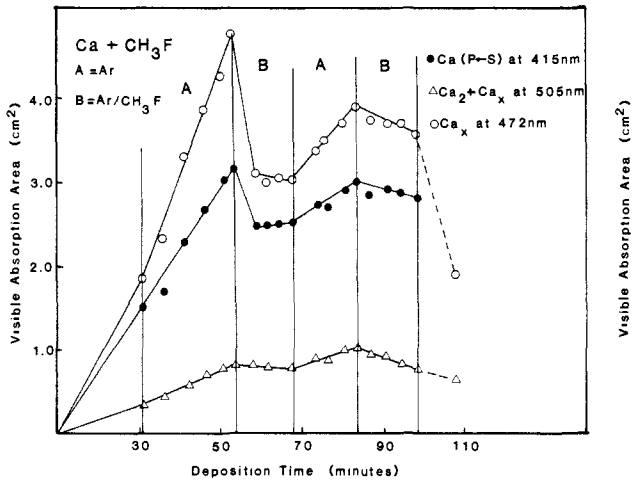

Figure 4. Absorption areas vs. time for calcium species in argon (A) vs. argon/CH_3F (B).

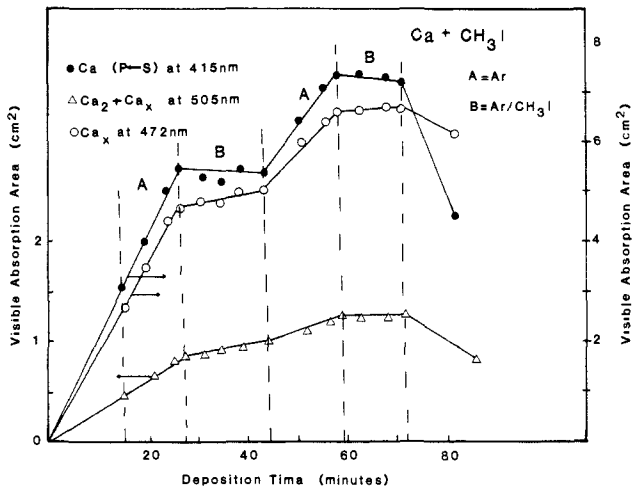

Figure 5. Absorption areas vs. time for calcium species in argon (A) vs. argon/CH_3I (B).

Figure 3 illustrates the actual spectra obtained for the Ca (P ← S) line. Similar plots were observed in all reactions where the atomic transitions grew rapidly in the presence of CH_3X (X = Cl, Br). No new bands were observed, and no change in band shape or position was observed.

Calcium/CH_3Br. These results were almost identical with those of the calcium/CH_3Cl case except that the growth rate for the Ca (P ← S) transition was not quite as great with CH_3Br as with CH_3Cl, or 300 vs. 400% at the same reaction time.

No new product peaks were observed in this experiment, and all bands decreased rapidly upon annealing.

Calcium/CH_3F. Figure 4 shows the results of calcium vapor codeposited with CH_3F and argon. In this case two new peaks were observed at 492 and 458 nm, which are found only in the presence of CH_3F. From the plot it can be seen that the atom and cluster peaks behaved similarly; they increase in argon, but diminish in argon/CH_3F.

Calcium/CH_3I. Figure 5 shows the Ca/CH_3I system. It is clear that all species Ca, Ca_2, and Ca_x were consumed by CH_3I. No new absorptions were observed.

Calcium/CH_4. With CH_4 we observed very different behavior as compared with CH_3X. The presence of CH_4 had little effect on band growth for Ca, Ca_2, or Ca_x. Even with pure CH_4 similar growth patterns were observed.

Magnesium. Literature background and the absorption spectrum for magnesium species were discussed earlier.[1] Extension of these studies for magnesium with CH_3Cl, CH_3F, CH_3I, and CH_4 are now reported.

Magnesium/CH_3Br. Our earlier work was reproduced showing that the Mg atom transitions at 281 and 285 nm grew more rapidly in the presence of CH_3Br (0.6% CH_3Br in argon). However, Mg_2 bands at 370 and 264 nm and the Mg_3 band at 345 nm stopped growing and decreased slightly with CH_3Br present.

Magnesium/CH_3I. All bands due to cluster species (Mg_2, Mg_3, Mg_4) had a retarded growth rate in the presence of CH_3I and actually decreased slightly. However, the Mg atomic transition growth rate increased in the presence of CH_3I. In other words, the same behavior as with CH_3Br was observed. Annealing caused a rapid decrease in all absorptions.

Magnesium/CH_3Cl. Interestingly, atomic bands and cluster bands behaved identically, that is, growth in argon and similar growth in CH_3Cl/argon.

Magnesium/CH_4. The same results as with magnesium + CH_3Cl were observed: very little change in band growth rate in the presence or absence of CH_4. Identical results were found with calcium + CH_4 noted earlier.

Magnesium/CH_3F. In this case new results were obtained. The atomic absorption lines growth rates changed very little throughout the experiment. Erratic growth rates for Mg_2 bands were observed, while band growth rates due to Mg_3, Mg_4, and Mg_x were retarded in the presence of CH_3F.

Discussion

Since calcium and magnesium vapor are almost completely monoatomic,[9] cluster species must form by M atom agglomeration during the brief codeposition/freeze-down period.[10] Thus, formation of clusters M_2–M_x is a kinetic phenomenon under matrix conditions.[11] And, as in our previous work,[1] we believe the different behavior of M atoms vs. M_2, M_3, and M_x can be explained on a kinetic/chemical reactivity basis. First, however, we should review some key points: (1) earlier infrared work by Ault[12] and in our laboratory[13] has indicated that oxidative addition reactions with CH_3X and magnesium/calcium species do occur, although the spectra are not characteristic enough for exact structure assignments. As would be expected a reactivity trend $CH_3I > CH_3Br > CH_3Cl > CH_4$ was found (CH_3F was not studied). (2) Second, we must deal with the fact that M atom isolation is greatly enhanced by the presence of CH_3Cl or CH_3Br. Three considerations come to mind: (a) since the presence of CH_3X does not change the position of surviving UV–vis bands, we do not believe CH_3X acts as a weakly interacting trap (CH_3X···M) for Mg or Ca atoms;[1] (b) there is the possibility that oxidative addition products CH_3M_xX are unstable and a M atom is ejected (e.g., $CH_3Ca_3X \rightarrow CH_3Ca_2X + Ca$); or finally, (c) the atom isolation enhancement may be strictly a kinetic phenomenon. Thus, our data could be explained in the following way using CH_3Br as an example. With CH_3Br, Ca and Mg atoms are unreactive under these low-temperature conditions. However, dimers and higher clusters of calcium and magnesium are reactive and are consumed by CH_3Br. Their consumption at the moment of their formation removes a pathway for M atom loss (further agglomeration). Therefore, in the presence of CH_3Br, M atom isolation would be enhanced:

$$\text{Ca + argon} \xrightarrow{k_1} \text{Ca atoms isolated/frozen} \quad (1)$$

$$\text{Ca + Ca} \xrightarrow{k_2} \text{Ca}_2 \quad (2)$$

$$\text{Ca + Ca}_2 \xrightarrow{k_3} \text{Ca}_x \ (x \text{ probably} = 3) \quad (3)$$

$$\text{Ca + CH}_3\text{Br} \rightarrow \text{no reaction} \quad (4)$$

$$\text{Ca}_2 + \text{CH}_3\text{Br} \rightarrow \text{CH}_3\text{Ca}_2\text{Br} \quad (5)$$

$$\text{Ca}_x + \text{CH}_3\text{Br} \rightarrow \text{CH}_3\text{Ca}_x\text{Br} \quad (6)$$

(9) Klabunde, K. J. *Chemistry of Free Atoms and Particles*: Academic Press: New York, 1980; pp 34, and references therein.
(10) Moskovits, M.; Ozin, G. *Cryochemistry*; Wiley: New York, 1976; p 395.
(11) (a) Kundig, E. P.; Moskovits, M.; Ozin, G. A. *Nature (London)* **1975**, *254*, 503–504. (b) Moskovits, M.; Hulse, J. E. *J. Chem. Soc., Faraday Trans.* **1977**, *73*, 471–484.
(12) Ault, B. S. *J. Am. Chem. Soc.* **1980**, *102*, 3480–3484.
(13) Tanaka, Y.; Davis, S. C.; Klabunde, K. J. *J. Am. Chem. Soc.* **1982**, *104*, 1013–1016.

Table II. Reactivities of Calcium and Magnesium Species with Alkyl Halides under Matrix Isolation Conditions

	Metal Species[a]							
alkyl halide	Ca	Ca_2	Ca_x	Mg	Mg_2	Mg_3	Mg_4	Mg_x
CH_3I	yes	yes	yes	no	yes	yes	yes	yes
CH_3Br	no	yes	yes	no	yes	yes		yes
CH_3Cl	no	yes	yes	no	no		no	no
CH_3F	yes	yes	yes	no	no	no	yes	yes
CH_4	no	no	no	no	no	no		

[a] "Yes" indicates that this species was consumed by CH_3X. "No" indicates that it was not. A blank means the spectral data were not good enough to determine reactivity.

Table III. Bond Strengths of Diatomic MX Species Compared with H_3C-X[a]

species	bond strength (kcal/mol)	species	bond strength (kcal/mol)
Ca-I	63 ± 2.5	Mg-Cl	78.3 ± 0.5
H_3C-I	56.3 ± 1	Ca-F	126 ± 5
Mg-I	~68	H_3C-F	108 ± 3
Ca-Br	74.3 ± 2.2	Mg-F	110.4 ± 1.2
H_3C-Br	70.0 ± 1.2	Ca-H	40.1
Mg-Br	78.2	H_3C-H	105.1 ± 0.15
Ca-Cl	95 ± 3	Mg-H	30.2 ± 0.7
H_3C-Cl	95 ± 7		

[a] *Handbook of Chemistry and Physics*, 65th ed.; CRC Press: Boca Raton, FL, 1984-85; pp. F171-F181; also 60th ed.; CRC Press: Cleveland, OH, 1980; pp F220-F224.

Thus, when CH_3Br is present the concentration of Ca_2 goes down, so the rate of reaction 3 becomes very small and process 1 becomes more favored; therefore, the rate of M atom isolation increases. (This argument assumes that the *products* of Ca_2 and Ca_x reactions with CH_3Br do not react at any appreciable rate with Ca atoms).

Interpretations of key points 2b and 2c require that our results be due to a higher chemical reactivity of M clusters as compared with M atoms. Differentiating 2b and 2c might be possible by matrix kinetic studies. However, this requires quantitative information about product growth. Unfortunately, UV-vis bands for products were not observed and are apparently broadened beyond recognition. Only qualitative rates of consumption of M atoms, M_2, M_3, and M_x could be obtained from our spectral data. So, even though we quantitatively monitored M vapor deposition, we were not able to successfully carry out kinetic studies.

Summary of Atom/Cluster Reactivities

Table II summarizes the reactivities of calcium and magnesium species. Note the trends. The most chemically active halide is CH_3I, and it reacted with all species except Mg atoms; CH_3Br reacted with only cluster species; CH_3Cl reacted with only calcium cluster species; CH_3F reacted with all calcium species and only larger magnesium species; and CH_4 reacted with none.

Although CH_3F is somewhat anomalous and will be discussed more later, the general reactivity trends are: $Ca_x \approx Ca_2 > Mg_x \approx Mg_4 > Mg_3 \approx Mg_2 > Ca > Mg$; $CH_3I > CH_3F > CH_3Br > CH_3Cl$.

Explaining Reactivities

Bond Strengths. Table III lists the known bond strengths of relevant diatomic species compared with known carbon-halogen bond strengths. From these data it is easy to see why magnesium atoms do not react with CH_3F or CH_3Cl. Also, it is reasonable that both calcium and magnesium species are unreactive with CH_4.[14]

In the cases where reactivity was observed, bond strength considerations are favorable or at least marginal. Thus, it appears that if thermodynamic considerations are at least reasonable, reactions are possible. In such cases, whether reactions occur or not depends on other factors.

Ionization Potentials and M-M Bond Strengths. In earlier work we proposed that the ionization potential (IP) of the metal atoms and clusters is an important parameter in determining reactivities.[13] Thus, Al atoms, which have an abnormally low first IP, were found to be highly reactive with CH_3X. Electron transfer or partial electron transfer from the metal species to CH_3X may immediately precede bond breaking:

$$Al + CH_3Br \rightarrow [CH_3Br^-Al^+] \rightarrow CH_3AlBr$$

Similar arguments pertain to the current work. Metal clusters generally have lower IPs than atoms;[15] for example, compare Mg atom IP = 7.6 eV and Mg_2 IP = 6.7 eV.[16] Also, the Mg-Mg bond strength is 1.2 kcal/mol, while ionized $[Mg-Mg]^+$ has a bond strength of 23.4 kcal. These data reinforce our earlier proposal, with theoretical support,[17] that Mg_2 may be more reactive than Mg atoms because: (a) Mg_2 can more easily transfer an electron to initiate the reaction proces, and (b) the logical product CH_3MgMgX should have a comparatively strong Mg-Mg bond; therefore, when Mg_2 reacts actually three bonds are made or strengthened: C-Mg, X-Mg, and Mg-Mg.

Similar considerations hold for Mg_3, Ca_2, Ca_3, and higher clusters.

At this point one may reasonably ask, "What is the driving force for electron transfer since electron affinities of CH_3X are relatively low?" The answer may lie in the ion-pair stabilization that is gained in the solid matrix. Electron transfer strengthens M-M bonding, and a Coulombic ionic attraction between the product $M_x^+CH_3X^-$ species would be present. This ionic stabilization could compensate for the mismatch in IP of the metal species (~6 eV) vs. the electron affinity of CH_3X (~1 eV).[18]

Steric or Orbital Overlap Considerations. A possibility that should also be considered is that M_2 or M_3 may be able to form a more favorable transition state; i.e., four-centered:

Experimentally, we cannot differentiate this possibility from others mentioned, and we await further theoretical approaches to this problem.

The CH_3F Case. From Table II we see that CH_3F appears to be even more reactive toward Ca species than CH_3Cl or CH_3Br. This seemingly anomalous behavior is reasonable if the data for Table III are considered. Note that reactions only take place if the diatomic bond strengths of M-X are equal to or exceed that of C-X. In the case of CH_3F the C-F bond strength is about the same as that of Mg-F, but is considerable smaller than that of Ca-F. The same trend is found for C-Cl vs. Ca-Cl and Mg-Cl. These data then clarify the reactivity trends found.

Another interesting finding with CH_3F is that with magnesium only the larger clusters Mg_x and Mg_4 appeared to react while Mg_3, Mg_2, and Mg did not. This is one of the clearest examples showing that reactivity is a function of cluster size. It is also interesting to note that Mg_4 behaves uniquely in this system. Its unusual spd hybridization appears to play a role in its reactivity, as compared with Mg_2 and Mg_3.[19]

The Ca/CH_3F case was the only combination where new peaks were observed (492 and 458 nm). These bands were very dependent upon CH_3F concentration and increased sharply in the presence of CH_3F, but decreased rapidly in its absence. Annealing caused a decrease in the intensity of these peaks at rates similar to the calcium atoms and clusters. This behavior would probably

(14) McCaffrey, J. G.; Parris, J. M.; Ozin, G. A.; Breckenridge, W. H. *J. Phys. Chem.* **1985**, *89*, 4945-4950.

(15) Rohlfing, E. A.; Cox, D. M.; Kaldor, A.; Johnson, K. H. *J. Chem. Phys.* **1984**, *81*, 3846-3850.

(16) Po, P. L.; Porter, R. F. *J. Phys. Chem.* **1977**, *81*, 2233-2236.

(17) (a) Jasien, P. G.; Dykstra, C. E. *J. Am. Chem. Soc.* **1983**, *105*, 2089-2090. (b) Jasien, P. G.; Dykstra, C. E. *Ibid.* **1985**, *107*, 1891-1895.

(18) It is difficult to predict the ion-pairing energy without knowning the distance between the ions, but they should remain quite close in a frozen matrix, and so attraction could be quite large.

(19) Chiles, R. A.; Dykstra, C. E.; Jordan, K. D. *J. Chem. Phys.* **1981**, *75*, 1044.

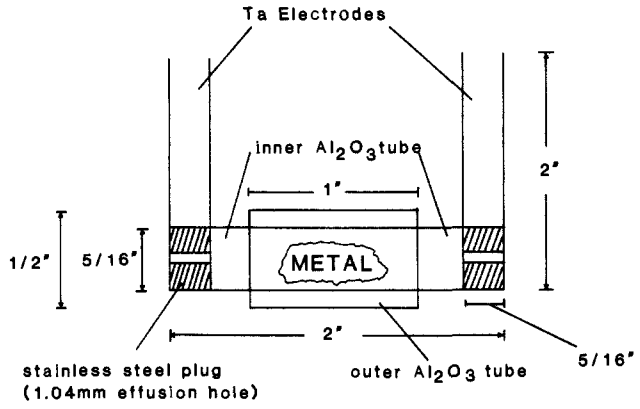

Figure 6. Modified Knudsen cell furnace used in matrix isolation experiments.

not be expected of oxidative addition products, and without further information we cannot give an interpetation as to the structures responsible for these bands.

Conclusions

Table II summarizes our findings and indicates that: (a) M_2, M_3, M_4, M_x species are more reactive than atoms (M = Mg and Ca), and this finding is supported experimentally (this work) and theoretically;[17] (b) Ca species are more reactive than Mg species; (c) the general reactivity trends is $Ca_x \approx Ca_2 > Mg_x \approx Mg_4 > Mg_3 \approx Mg_2 > Ca > Mg$ [note that larger clusters are usually more reactive than smaller ones, which in turn are more reactive than atoms]; (d) the CH_3X reactivity trend with these metal species is $CH_3I > CH_3F > CH_3Br > CH_3Cl$, and is reasonable based on the bond strenth data from Table III comparing diatomic M–X vs. C–X; and (e) electron transfer may be an important step leading to bond breaking, whereby lower IPs lead to higher reactivities.

Experimental Section

Apparatus. Our matrix isolation unit is a modified version of that reported by Hauge, Margrave, and their co-workers.[20] It is designed so that the matrix chamber can be moved freely into and out of a Beckman IR-12 spectrophotometer and a Cary 14 UV–vis spectrophotometer. The mounting allows both reflectance and absorption/transmission studies to be carried out. The complete design and specifications have been described previously.[21] The unit is cooled by an Air Products Displex closed cycle helium refrigerator, Model CSW202. Fine temperature control is possible using an Air Products APD-E digital temperature indicator/controller. A cold cathode gauge and monitor (Kontes/Martin) were used to measure the background pressure. This pressure was approximately 4×10^{-6} torr before vaporization started and remained about 2×10^{-5} torr during the experiment.

The furnace is a modified Knudsen cell design. The exact dimensions are illustrated in Figure 6. It was made by cutting a 2 in. × $^5/_{16}$ in. o.d. pressed Al_2O_3 tube with a wall thickness of 0.05 in. The tube was then wrapped with 25-μ Ta foil and spot welded along the seam. Next an 0.5 in. o.d. Al_2O_3 sleeve 1 in. long with a 0.055-in wall thickness was slid over the Ta-wrapped tube. This sleeve was also wrapped in 25-μ Ta foil and served as a heat shield to reduce the amount of radiant energy escaping from the furnace. The outer sleeve was centered in the middle of the Al_2O_3 tube. At each end of the furnace there was a $^5/_{16}$ in. wide piece of 0.5-mm Ta metal which was wrapped around the end of the furance and spot welded. These served as electrodes for the furnace and extended perpendicular to the furnace axis about 2 in. The metal used for vaporization was then placed inside the inner Al_2O_3 tube approximately in the center. Each end of the furnace was then fitted with a stainless steel plug in which there was a 1.04-mm aperture. These openings allowed metal vapor to escape in one direction toward a cold KBr (25 mm × 4 mm) window which was used for spectroscopic detection, and in the opposite direction toward a quartz crystal microbalance. This microbalance was attached to a digital frequency counter (Data Precision No. 335845) which allowed quantitative measurement of metal deposited.[22]

A chromel–alumel thermocouple was inserted between the two Al_2O_3 tubes in the furnace and connected to a Type K digital thermometer. The distance from one Knudsen cell effusion hole to the KBr window was 9 cm, and from the other exit to the microbalance was 11 cm.

The microbalance is made of a quartz piezoelectric sensor crystal (Airco Temescal Model Sc-8009) with a gold plating. The crystal oscillates at a frequency of ≈6.0 MHz. As metal deposits on the crystal face, the oscillation frequency decreases. The frequency shift caused by the deposition of metal has been theoretically described by Sauerbrey.[23] The amount of metal deposited on the crystal can be calculated.[22,24]

Amounts of Metal Vaporized. Typical furnace temperatures were between 360 and 480 °C for Mg and 460 and 560° for Ca. Total vaporization periods were about 12 h. However, with the use of a shutter, which blocked the KBr window during spectroscopic observation and during periods of instrument adjustment, the actual vaporization time for the metal flux in contact with KBr window was reduced to between 1 and 3 h. Using the proper equations,[22,24] we calculated the grams of metal being deposited per hour onto the microbalance and thus onto our KBr window. The following is a model calculation for a calcium deposit. The microbalance frequency was decreasing at a rate of 0.2405 Hz/h. The thickness of the crystal and film was assumed to be very near that of the crystal alone in the beginning hours of the vaporization.

$$\Delta g = A\rho(Q)T\Delta f/f$$

$$\Delta g = (1.40\ \text{cm}^2)(2.5\ \text{g/cm}^3)(0.028\ \text{cm})(0.2405\ \text{Hz/h})/(5881.38\ \text{Hz})$$

$$\Delta g = 4.0 \times 10^{-6}\ \text{g/h}$$

$$\frac{4.0 \times 10^{-6}\ \text{g/h}}{40.09\ \text{g/mol}} = 9.9 \times 10^{-8}\ \text{mol/h} = 9.9 \times 10^{-5}\ \text{mmol/h}$$

In our experimental design, the KBr window was 2 cm closer to the furnace effusion hole than the microbalance. By replacing this KBr window with a second microbalance, it was determined that the window accumulated three times the amount of metal than the first microbalance. Assuming that all the metal which hit the window was trapped, we calculated the actual amount of metal being deposited on the KBr window as being 3.0×10^{-4} mmol/h for calcium and 5.0×10^{-5} mmol/h for magnesium. During each experiment, the matrix gas flow was adjusted to 1.6 mmol/h. This resulted in a matrix gas/metal ratio for 5.3×10^3 for Ca and 3.2×10^4 for Mg.

Chemicals and Gases. The magnesium (Alfa Products, 99.99%) and calcium were outgassed at elevated temperatures prior to depositions. Methyl iodide (Aldrich 99%), methyl bromide (Linde 99.5%), methyl chloride (Matheson 99.5%), and methyl fluoride (Matheson 99%) were frozen at liquid N_2 temperature and volatile impurities were pumped off. This degassing cycle was carried out several times for each halide. The methane (Linde, 99%) was passed through degassed molecular sieves (13×) at 77 °K to remove unwanted water and oxygen. The argon (Linde, 99.99%e was exposed to a copper catalyst (Chemical Dynamic R3-11) to scavenge any unwanted oxygen. Argon and each alkyl halide were mixed in a 3.5-L gas bulb using convection heating. The dilution ratio of Ar to CH_3X was 152:1 in all cases.

Spectroscopic Measurements. These were made using a Cary 14 UV–vis spectrophotometer. A clean KBr window served as a reference sample. The slit width was automatically varied between 0.04 and 0.1 mm. Typically scans were made from 650 to 400 nm for Ca and from 400 to 240 nm for Mg. During each separate experiment, however, periodic scans were carried out from 650 to 240 nm in search of any new product or impurity peaks. The scan speed was set at 0.25 nm/s. After an experiment was completed, the matrix appeared almost transparent with a light brown tint.

In each initial experiment, the matrix gas flow rate, the temperature of the matrix, and the deposition rate of the metal were all systematically varied to achieve optimum isolation conditions. When these conditions were correct, absorptions due to M, M_2, and M_x were observed and growth rates of each species were recorded. Growth was monitored by determining the peak areas using an Apple computer with Graphics Tablet software. UV–vis band assignments were made based on prior literature which was discussed earlier in this paper.

Typical Experimental Procedure. Over several hours the system was pumped to $< 4 \times 10^{-5}$ torr. Water flow to the electrodes and cryocooler was started and the KBr window cooled to 9 K. During this time (ca. 1 h) the furnace was slowly warmed to the vaporization temperature (the KBr window was rotated 90° and protected by a shutter to prevent any premature metal deposition). The microbalance was activated and Ar

(20) Hauge, R. H.; Kauffman, J. W.; Margrave, J. L. *J. Am. Chem. Soc.* **1980**, *102*, 6005–6011, and references therein.
(21) Davis, S. C. Ph.D. Thesis, University of North Dakota, 1980.
(22) Wolter, A. R. *J. Appl. Phys.* **1965**, *36*, 2377–2381.
(23) Sauerbrey, G. *Z. Phys.* **1959**, *155*, 206.
(24) Ozin, G. A.; Moskovits, M., In ref 10, p 54.

deposition commenced. Then the KBr window was rotated into place and metal and Ar codeposition were begun. After deposition for a desired period of time the window was rotated 90°, protective shutter in place, and Ar flow stopped. A spectrum was recorded. This cycle was carried out as many times as necessary to determine the growth rate of M, M_2, M_3, and M_x species.

When changing the matrix gas from Ar to Ar/CH_3X or vice versa, the following adjustments were made. First the valve on the Ar gas bulb was closed. Then both gas valves were closed and any gaseous Ar in the apparatus was pumped away. Both gate valves were again opened and background pressure was allowed to stabilize. The valve on the Ar/CH_3X gas bulb was then opened and the flow rate into the matrix chamber controlled by the needle valve. The deposition procedure was then identical with that stated above. (Note that the furnace remained at constant vaporization temperature throughout all manipulations; metal vapor was collected on the shutter while spectra were being recorded or other manipulations made.)

When the deposition cycles were complete, an annealing experiment was carried out by first closing the needle valve and any opened gas bulb valves. The window was then rotated into the spectroscopic observation path and the annealing temperature was adjusted using the Digital temperaure controller. When the annealing time was complete, the KBr window was cooled back down to 9 K and a spectrum recorded.

When the experiment was completed, the shut-down procedure began by turning off the diffusion pump and isolating it from the rest of the system by closing the appropriate gate valve. Then the furnace as well as cryocooler were were shut off. The circulating water for the diffusion pump, electrodes, and cryocooler was left on until the system was adequately equilibrated. It took approximately 6 h for the KBr window to warm to room temperature. At this time the window could be changed and another experiment carried out.

Acknowledgment is made to the donors of the Petroleum Research Fund, administered by the American Chemical Society, for support of this work. Program support for the National Science Foundation is also greatly appreciated.

Registry No. Ca, 7440-70-2; Ca_2, 12595-85-6; Mg, 7439-95-4; Mg_2, 29904-79-8; Mg_3, 72673-77-9; Mg_4, 73767-50-7; CH_3Cl, 74-87-3; CH_3Br, 74-83-9; CH_3F, 593-53-3; CH_3I, 74-88-4; CH_4, 74-82-8.

Is Butatrienone ($H_2C=C=C=C=O$) Kinked?

Ronald D. Brown,* Peter D. Godfrey, Martin J. Ball, Stephen Godfrey, Donald McNaughton, Martin Rodler, Burkhard Kleibömer, and Robert Champion

Contribution from the Department of Chemistry, Monash University, Clayton, Victoria, Australia 3168. *Received May 19, 1986*

Abstract: We have studied by microwave spectroscopy the vibrational satellite series of H_2C_4O and D_2C_4O that is associated with the lowest out-of-plane bending mode ν_{15}. From a semirigid bender analysis, including data of up to $\nu_{15} = 5$, it is concluded that a shallow single-minimum potential is responsible for the observed pattern. Parallel to this study we carried out 6-31G** MO calculations, which yielded a barrier to planarity of only 5.6 cm^{-1}, in contrast to a value of 433 cm^{-1} obtained in a previous study by Farnell and Radom. We conclude that butatrienone is *not* kinked in its equilibrium configuration.

The cumulenones, H_2C_nO, are compounds of particular interest in structural chemistry because at least two members of the series display structural features that are in conflict with the predictions of ab initio molecular orbital calculations. For one of these there is also conflict with classical structural theory which implies that all members of the series have a symmetrical planar C_{2v} structure, and this is known to be the case for formaldehyde and ketene. When the microwave spectrum of propadienone was first studied[1] there were indications that it might not have C_{2v} symmetry, and this has subsequentally been demonstrated conclusively in a series of spectral studies.[2-5] Parallel theoretical studies of its structure based on ab initio molecular orbital calculations taken to the Hartree-Fock level with substantial basis sets (such as 6-31G**) erroneously predicted a symmetrical geometry.[6] It was only when electron correlation was included that the kinked in-plane geometry (Figure 1) was correctly predicted.[7,8]

When butatrienone was first characterized,[9] the spectra of the main species and of two isotopic variants were consistent with that of a symmetrical C_{2v} structure. Some recent molecular orbital calculations[10] that included electron correlation however have predicted that butatrienone is strongly kinked, as shown in Figure 2. The predicted barrier to the symmetrical shape (433 cm^{-1} at the MP3/6-31G level calculation) was higher than that for propadienone (167 cm^{-1} at the MP3/6-31G level). We believe, however, that the way in which these MO calculations were carried out does not lead to reliable results and have consequently performed additional calculations reported below.

The previous experimental demonstration that butatrienone is not kinked but is planar, in clear disagreement with MO theory published until now, was mainly dependent on the value of the inertial defect and thus subject to the appreciable uncertainty in I_a which cannot be determined with high precision by microwave spectroscopy alone for this molecule. It therefore seemed desirable to establish the geometry of butatrienone more precisely by studying the out-of-plane vibrations directly via the vibrational satellites in the microwave spectrum. Thus further study, and finally the use of the semirigid bender model analogous to that recently reported for propadienone,[4,5] is reported here.

Experimental Section

The microwave spectrometer involved a microprocessor-controlled synthesized microwave source designed and constructed at Monash University. The synthesizer was referenced to our laboratory frequency standard and the Australian frequency standard at C.S.I.R.O. Division of Applied Physics. The microwave oscillator was a Hewlett Packard 8690 series plug-in BWO. The cell was a 3-m length of G-band waveguide, Stark modulation being at 6.525 kHz. The spectral data were collected and reduced in a Sperry-Univac V75 computer system.

Double resonance (microwave-radio frequency) studies were performed by locking the microwave source to the center frequency of an absorption line and feeding a radio frequency signal into the Stark septum of the cell. The radio frequency signal was swept through the double-

(1) Blackman, G. L.; Brown, R. D.; Brown, R. F. C.; Eastwood F. W.; McMullen, G. L. *J. Mol. Spectrosc.* **1977**, *68*, 488-491.
(2) Brown, R. D.; Godfrey, P. D.; Champion, R.; McNaughton D. *J. Am. Chem. Soc.* **1981**, *103*, 5711-5715; **1982**, *104*, 6167.
(3) Brown, R. D. *J. Mol. Struct.* **1983**, *97*, 293-302.
(4) Brown, R. D.; Champion, R.; Elmes, P. S.; Godfrey, P. D. *J. Am. Chem. Soc.* **1985**, *107*, 4109-4112.
(5) Brown, R. D.; Godfrey, P. D.; Champion R. *J. Mol. Spectrosc.*, to be published.
(6) Radom, L. *Aust. J. Chem.* **1978**, *31*, 1-9.
(7) Farnell, L.; Radom, L. *Chem. Phys. Lett.* **1982**, *91*, 373-377.
(8) Taylor, P. R. *J. Compt. Chem.* **1984**, *5*, 589-597. Brown, R. D.; Dittman R. D. *Chem. Phys.* **1984**, *83*, 77-82.
(9) Brown, R. D.; Brown, R. F. C.; Eastwood, F. W.; Godfrey, P. D.; McNaughton, D. *J. Am. Chem. Soc.* **1979**, *101*, 4705-4708.
(10) Farnell, L.; Radom, L. *J. Am. Chem. Soc.* **1984**, *106*, 25-28.

0002-7863/86/1508-6534$01.50/0